The Brownian Integral Kernel:
A New Kernel for Modeling Integrated Brownian Motions

Béla H. Böhnke[1][0000−0002−3779−3409] bela.boehnke@kit.edu, Edouard Fouché[2][0000−0003−0157−7648], and Klemens Böhm[1][0000−0002−1706−1913]

[1] Karlsruhe Institute of Technology (KIT) IPD, Kaiserstraße 12, Karlsruhe, 76131, Baden-Würtemberg, Germany
[2] Siemens Deutschland – Work originated while at KIT, Werner-von-Siemens-Straße 1, München, 80333, Bayern, Germany

Abstract. Brownian motion is widely used to model random processes across various domains. However, many practical scenarios only provide aggregated data over time intervals, rather than direct measurements of the underlying process. This poses significant challenges for accurate modeling, as conventional Brownian kernels are not designed to account for the uncertainty introduced by these aggregates. We introduce the *Brownian integral kernel* (BIK), the first analytical kernel specifically developed to model aggregated data from Brownian motion. Through extensive experiments on synthetic and real-world datasets, we demonstrate the BIK's superiority in prediction accuracy, uncertainty estimation, and data synthesis compared to existing Kernels. To support adoption, we provide a Python implementation[3] compatible with GPy, along with all code and data to reproduce our experiments.

Keywords: Integral Measurements· Learning from Aggregated Data· Integrated Brownian Motion· Gaussian Process Regression· Kernels

1 Introduction

Brownian motion (Figure 1a) is central to modeling various physical and technological processes, such as: (1) The movement of particles in a fluid [7]. (2) The movement and loosening of machine elements due to vibration [13]. (3) The behavior of financial and other markets [17], population behavior and effects. (4) The load profile of electrical grids where producers and consumers with varying loads are plugged in or out of the grid at any time. These processes often involve stochastic uncertainties, which are effectively modeled using Gaussian processes and Brownian kernels [4], enabling synthesis of process data, regression of real-world data with associated uncertainty, and the combination of both, i.e., synthesis of data from partially conditioned models.

However, in many real-world scenarios, data collection pipelines contain "integrators" that implicitly or explicitly aggregate data over time intervals [19]

[3] git: https://github.com/bela127/Brownian-Integral-Kernel

(Figure 1b). Direct observation of the quantity of interest is not possible in such scenarios. Examples include sensors with inherent integration properties (e.g., temperature sensors with heat capacity) or practical constraints (e.g., smart meters providing 15-minute aggregated load data for value privacy). This aggregation obscures the underlying behavior and increases uncertainty, which conventional Brownian kernels cannot model accurately (Figure 1c). For instance, load forecasting requires precise variance estimation to manage short-term peaks in energy consumption [8, 18, 28]. Without this, providers risk grid instability or legal penalties due to insufficient capacity [3]. Similar problems arise in other domains like disease monitoring and simulation [34]. As emphasized by [5], the importance of integral kernels for modeling integrating processes is undisputed in many fields.

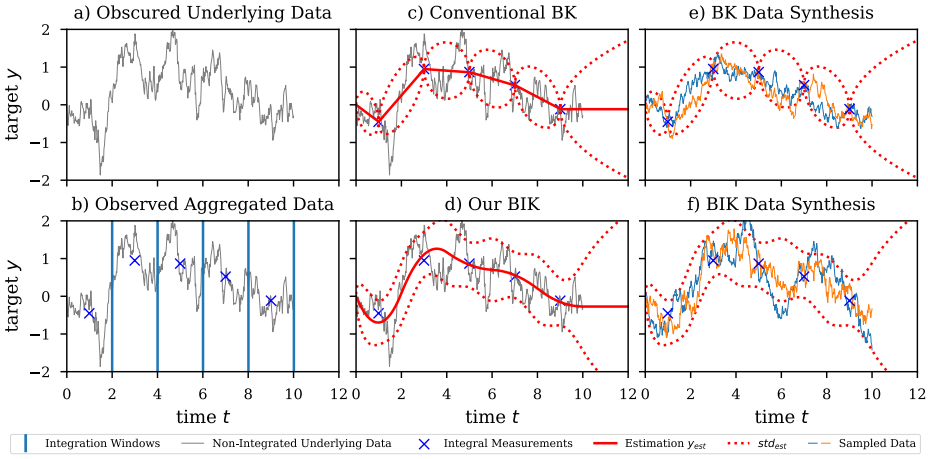

Fig. 1. Comparison of modelling and synthesis of integrated Brownian data with the conventional Brownian Kernel (BK) and our *Brownian Integral Kernel (BIK)*.

While a few integral kernels exist (e.g., RBF Integral Kernel), they are often computationally expensive or lack a direct connection to physical processes, making them unsuitable for integrated Brownian motion.

To address these challenges, we derive the *Brownian Integral Kernel (BIK)*, a novel analytical solution for modeling aggregated data from Brownian motions. The BIK accurately estimates variance and supports Gaussian process regression, enabling better predictions and uncertainty quantification (Figure 1d), as well as data synthesis (Figure 1f). We validate its performance through extensive experiments on synthetic and real-world datasets. Further, to foster accessibility, we provide a Python implementation of the BIK compatible with the widely used [9] framework for Gaussian Process modeling. For brevity of this paper, we provide proofs, theoretical findings, and additional experiments in our extensive Supplementary material.

2 Related Work

Gaussian processes (GPs) are a standard tool for modeling continuous processes, offering flexible kernels that enable accurate regression, uncertainty quantification, and data generation [4]. Their robustness to overfitting and scalability make them well-suited for both small and large datasets [6]. A key strength of GPs is their use of kernel functions, which allow for modeling complex, non-linear relationships without explicit parametric assumptions. The general workflow for using GPs is outlined in Algorithm 1:

Algorithm 1 Generic Use-Case of a Gaussian Processes

1: **Input:** Training data $\mathbf{t}_{\text{train}}$, $\mathbf{y}_{\text{train}}$, Test data $\mathbf{t}_{\text{test}}$
2: **Output:** Predicted mean $\mu(\mathbf{t}_{\text{test}})$, uncertainty $\sigma(\mathbf{t}_{\text{test}})$, generated data $\mathbf{y}_{\text{gen}}$
3: **Step 1: Kernel Selection.** Choose a kernel function $k(\cdot, \cdot)$ (e.g., RBF, Matérn, our BIK, etc., or combination).
4: **Step 2: Training.** Train the Gaussian process model on $\mathbf{t}_{\text{train}}$, $\mathbf{y}_{\text{train}}$ using the kernel $k(\cdot, \cdot)$. Learn hyperparameters θ of the kernel by maximizing the log marginal likelihood.
5: **Step 3: Prediction and Uncertainty Estimation.** For test points $\mathbf{t}_{\text{test}}$, compute the posterior mean $\mu(\mathbf{t}_{\text{test}})$ and variance $\sigma^2(\mathbf{t}_{\text{test}})$ using the trained model.
6: **Step 4: Data Generation from Posterior Distribution.** Sample from the posterior $\mathcal{N}(\mu(\mathbf{t}_{\text{test}}), \sigma^2(\mathbf{t}_{\text{test}}))$ to generate new data $\mathbf{y}_{\text{gen}}$.

Despite their strengths, conventional kernels face limitations when modeling aggregated data. The RBF Integral Kernel [5,29] lacks physical grounding, while numeric integration-based methods [20,33] and MCMC approximations [34] are computationally expensive. Spectral approximations [10,30] succeed for smooth kernels but fail for discontinuous ones like the Brownian kernel [22].

The Brownian kernel, in contrast, is closely tied to physical processes such as load profiles and market behavior. However, it assumes direct observations, limiting its utility for aggregated data. Efforts to adapt Kalman filters [12,15,24, 25,31,32,35,36] and integrate numeric methods [16,20] have resulted in problem-specific or approximate solutions. For more details, see the extended related work in Supp.Mat. 2

Some approaches are out of scope for this work. Time-discrete methods, such as Kalman filters, lack the continuous modeling required for integrated data, while extensions for time-continuous modeling [15, 32] require problem-specific transition functions. Methods like Support Vector Machines (SVMs) do not support uncertainty estimation, and neural networks lack efficient mechanisms for data generation and uncertainty quantification. These limitations make them unsuitable as baselines for this study.

This paper introduces the *Brownian Integral Kernel (BIK)*, an analytical solution for modeling aggregated data. The BIK directly relates to common physical processes and provides exact covariance estimation for integrated Brownian

motion, enabling efficient computation within standard GP frameworks while maintaining a direct connection to physical processes.

3 Problem Statement

For clarity and completeness, the detailed notation and fundamental definitions are provided in Supp.Mat. 1. Although the notation is designed to be intuitive and should become clear from the context, readers are encouraged to refer to Supp.Mat. 1 as needed for additional details.

We assume a data-generating process $B(t)$ that behaves like a Brownian motion. Some real processes that behave like this do not allow observation of their actual value $b(t)$ (realization) at time t. One can only observe average or integral measurements of $B(t)$, while the true value $b(t)$ remains unknown.

Definition 1. *An integral measurement $\mathcal{B}(s, e)$ is the integration over time t of measurements from $b(t)$ from start time s to end time e:*

$$\mathcal{B}(s, e) = \int_s^e b(t)\delta t.$$

Even if $b(t)$ follows a Brownian motion which is per definition erratic, integral measurements $\mathcal{B}(s, e)$ behave differently, this is because integration smoothes the values leading to a smoother function. In consequence the measured value $\mathcal{B}(s, e)$ is most certainly not the true value of the underlying process $b(t)$. However, a Brownian motion model, e.g., a Gaussian process with Brownian kernel $k_{ff'}(t, t') = v_b \cdot min(t, t')$ assumes that the observed data points are the true values. Fitting such a model on integral measurement $\mathcal{B}(s, e)$ gives the wrong predictive variance of zero at measurement locations. To obtain the correct covariance, i.e., to correctly model the additional variance due to integration, a new kernel is necessary.

4 The Brownian Integral Kernel

We propose to model the additional variance (described in the previous section) directly in a new kernel to solve the problem of mis-estimating the variance. Thus, this calls for a kernel that yields the covariance between two integrated time intervals of a Brownian motion. Following [5] we can derive this kernel by integrating the Brownian kernel:

Definition 2. *The Brownian integral kernel (BIK) is the two-time integration over time intervals (s, e) and (s', e') of the Brownian kernel:*

$$k_{\mathcal{F}\mathcal{F}'}((s, e), (s', e')) = v_b \cdot \int_{s'}^{e'} \int_s^e min(t, t')\delta t \delta t'.$$

This kernel generalizes the Brownian kernel to integral measurements by modeling the higher variance due to integration, which the Brownian kernel neglects. For intuition and proof of how integrating a kernel is equivalent to integrating the underlying process, please refer to Supp.Mat. 3. Further, a kernel needs to fulfill some properties, namely, it needs to be positive-semidefinite [26]. We provide proof for this property in Supp.Mat. 4.

Theorem 1. *The Brownian integral kernel admits the following solution:*

$$
\begin{aligned}
&k_{\mathcal{F}\mathcal{F}'}((s,e),(s',e')) = \\
&\qquad v_b \cdot \begin{cases}
\text{if } s \le s' < e' \le e: \\
\quad \mathcal{F}_{tt}((e',t),(s',e')) + \mathcal{F}_{tt'}(s',e') + \mathcal{F}_{t't'}((s,s'),(s',e')) \\
\text{if } s' < e' \le s < e: \\
\quad \mathcal{F}_{tt}((s,e),(s',e')) \\
\text{if } s' \le s < e' \le e: \\
\quad \mathcal{F}_{tt}((s,e),(s',s)) + \mathcal{F}_{tt}((e',e),(s,e')) + \mathcal{F}_{tt'}(s,t') \\
\text{if } s \le s' < e \le e': \\
\quad \mathcal{F}_{t't'}((s,s'),(s',e')) + \mathcal{F}_{t't'}((s',e),(e,e')) + \mathcal{F}_{tt'}(s',e) \\
\text{if } s < e \le s' < e': \\
\quad \mathcal{F}_{t't'}((s,e),(s',e')) \\
\text{if } s' \le s < e \le e': \\
\quad \mathcal{F}_{tt}((s,e),(s',s)) + \mathcal{F}_{tt'}(s,e) + \mathcal{F}_{t't'}((s,e),(e,e'))
\end{cases}
\end{aligned}
$$

, with $\mathcal{F}_{tt}, \mathcal{F}_{t't'}, \mathcal{F}_{tt'}$ being sub-parts of the primitive function:

$$\mathcal{F}_{tt}((l',u'),(l,u)) = \frac{1}{2}u^2 \cdot u' - \frac{1}{2}u^2 \cdot l' - \frac{1}{2}l^2 \cdot u' + \frac{1}{2}l^2 \cdot l', \tag{1}$$

$$\mathcal{F}_{t't'}((l',u'),(l,u)) = \frac{1}{2}u'^2 \cdot u - \frac{1}{2}l'^2 \cdot u - \frac{1}{2}u'^2 \cdot l + \frac{1}{2}l'^2 \cdot l, \text{ and} \tag{2}$$

$$\mathcal{F}_{tt'}(l,u) = \frac{1}{3}(u-l)^3 + (u-l)^2 \cdot l. \tag{3}$$

We provide a detailed proof of this derivation in Supp.Mat. 8.

The resulting kernel $k_{\mathcal{F}\mathcal{F}'}$ calculates the covariance between training data intervals, i.e., between two integrated time intervals. However, during inference, most users are interested in the predictive variance $k^{post}_{ff'}$.

Definition 3. *The predictive variance $k^{post}_{ff'}$ of a Gaussian process is a variance within the original space of the non-integrated Brownian motion. For a given point t', $k^{post}_{ff'}$ quantifies how likely a prediction $y_{t'}$ is equal to the unobserved ground truth $\hat{y}_{t'}$.*

The predictive variance $k^{post}_{ff'}$ is often used to quantify the uncertainty associated with predictions $y_{t'}$ [27]. To calculate it, we need to calculate the *partly integrated* covariance $k_{\mathcal{F}f'}$.

Definition 4. *The* partly integrated *covariance $k_{\mathcal{F}f'}$ is the covariance between an inference point t' (point in the original space of non-integrated Brownian motion) and an integration time interval (s, e). It is calculated as a one-time integration of $k_{ff'}$:*

$$k_{\mathcal{F}f'}((s,e),t') = v_b \cdot \int_s^e min(t,t')\delta t.$$

Theorem 2. *The* partly integrated *kernel admits the following solution:*

$$k_{\mathcal{F}f'}((s,e),t') = v_b \cdot \begin{cases} if\, t' \leq s < e: \\ \quad \mathcal{F}_t(t',s,e) \\ if\, s < t' < e: \\ \quad \mathcal{F}_{t'}(s,t') + \mathcal{F}_t(t',t',e) \\ if\, s < e \leq t': \\ \quad \mathcal{F}_{t'}(s,e) \end{cases}$$

with $\mathcal{F}_t, \mathcal{F}_{t'}$ as follows:

$$\mathcal{F}_t(t,l',u') = t \cdot u' - t \cdot l', \tag{4}$$

$$\mathcal{F}_{t'}(l',u') = \frac{1}{2}u'^2 - \frac{1}{2}l'^2. \tag{5}$$

We obtain this partly integrated covariance by one-time integration of $k_{ff'}(t,t')$. The proof follows directly from the proof of Theorem 1, see Supp.Mat. 8. Here, Equations 4 and 5 are an intermediate result (compare with Equations 1 and 2) from Supp.Mat. 8.

We can now calculate the predictive variance $k^{post}_{ff'}$ of the Gaussian process, according to [23] with the standard formula for Gaussian processes. Here we use matrix notation, where K_{ff}, K_{Ff}, K_{FF} is the matrix obtained by using the appropriate kernel $k_{ff'}(*,*), k_{\mathcal{F}f'}(*,*), k_{\mathcal{F}\mathcal{F}'}(*,*)$ and K^{post}_{ff} is the result matrix that corresponds to $k^{post}_{ff'}$:

Corollary 1.

$$K^{post}_{ff} = K_{ff} - K_{fF}K^{-1}_{FF}K_{Ff}.$$

5 Experimental Design

We derived the Brownian Integral Kernel (BIK) and highlighted its advantages over existing kernels.

To validate our findings, we compare the BIK in various scenarios against the Brownian Kernel (BK), the RBF Integral Kernel (RBFIK) from [5], and the Brownian Kernel with added white noise (BNK) [2, 14]. The comparisons assess prediction quality, variance estimation, and the plausibility of data generated by a GP conditioned on integral measurements.

5.1 Used Data

For our evaluation, we use data from multiple sources: **Synthetic data:** *Synth* from a Gaussian process with a Brownian Kernel and subsequent numeric integration. **Simulated data:** *Load* generated with a realistic and widely used data generator [21]. **Real-world data:** *Real* provided by a private household, *HIPE* using the High-resolution Industrial Production Energy (HIPE) data set [1], and *Stock*, using daily stock market prices from [11]. More details on the used data can be found in our Supp.Mat. 5. We provide all used datasets which are otherwise not easily accessible, together with the experiment code within our GitHub repository to facilitate reproducibility.

It is important to note that, contrary to the intuition of the name *load profile*, load profiles can have both positive and negative values due to generating nodes such as photovoltaic systems. Especially for short-term modeling of such load profiles, they behave Brownean-like because of randomly moving cloud cover [37]. For long-term modeling, one almost always has additional periodicity (day and night). However, the periods are usually much longer than 15 minutes, which is why they are not relevant for modeling uncertainty due to integration. Our kernel can be used for long-term modeling with standard kernel composition by just adding a periodic kernel. Yet such an extension is not necessary for evaluating the short-term uncertainty effects we are targeting.

5.2 Metrics

We evaluate multiple application-relevant aspects of the kernels. One is often interested in the prediction error. However, in our scenario (where one can only observe integrals of the ground truth but not the ground truth itself) predictions will always be close to the mean within the observed integration interval. Therefore, standard metrics such as Mean Square Error (MSE) are not meaningful when comparing the kernels. Instead, this scenario requires an evaluation that combines prediction and prediction uncertainty. For this, we use the Weighted Mean Absolute Error (WMAE):

Definition 5. *The WMAE quantifies the estimation quality considering the estimated likelihood $l_{GP}(t')$ of an estimation $y_{t'}$ vs the ground truth $\hat{y}_{t'}$:*

$$WMAE = \frac{1}{|\mathbf{T}|} \sum_{t' \in \mathbf{T}} l_{GP}(t') \cdot |y_{t'} - \hat{y}_{t'}|$$

with $\mathbf{T}$ being the set of test points.

The WMAE is an intuitive measure: The estimated likelihood $l_{GP}(t')$ quantifies for a prediction $y_{t'}$ how likely this prediction is. If the model is confident ($l_{GP}(t') \approx 1$) and the prediction is accurate, the WMAE is low. WMAE penalizes prediction errors more when the model is (wrongly) confident, and less when it is (correctly) uncertain. Note that we are interested in the likelihood per data point, thus it is not required to normalize the likelihood across all data points.

While the WMAE is relevant for the prediction accuracy, we can also directly evaluate the estimated uncertainty. For this, we calculate the variance of the ground truth within an integration interval and compare it with the estimated variance, which should be similar. We use the Mean Square Error MSE_{var} between true and estimated variance. Please note, that this metric is only meaningful in combination with the prediction error.

Finally, we evaluate whether the generated data (which is partially conditioned on observed integral measurements) matches the process assumptions: We know that the integral of the ground truth results in the observed integral measurement. Therefore, the integral of generated data should also result in the observed integral. Here, we calculate the Mean Absolute Error MAE_{int} between the integral measurement and the integral value of generated data. We calculate the integral value of generated data by sampling data at the same points in time used to calculate the ground truth integrals and then apply the same windowing procedure, i.e., summing all the resultant values within the integration time interval.

5.3 Experiment Procedure and Model

We evaluate each kernel using the same Gaussian process model. As a model, we use the standard GPy implementation [9]. We also train all configurations in the same way, using the GPy gradient-based maximum likelihood optimizer in its standard configuration [9]. In this configuration, the optimizer performs 5 independent optimization runs, each time with random start kernel parameters. The model then uses the parameters from the best run.

For each dataset, we repeat this procedure 20 times, each time with a different ground truth time series. We then calculate the mean and the variance across the runs of the respective metrics.

6 Evaluation

For brevity, we focus here on the quantitative experiments. However, we feature additional qualitative kernel comparisons and visualizations in Supp.Mat. 6. These are especially useful for domain experts who like to attain an intuitive/visual understanding of the superiority of the BIK against other kernels. Further, we provide an ablation study of process and kernel parameters in Supp.Mat. 7 , and a theoretical runtime analysis in Supp.Mat. 3.

A comparison of the different approaches, in Table 1, shows that BIK is superior to its competitors in every regard evaluated: The integral of generated data has at least 10 times lower MAE_{int} compared to all baselines. (The RBFIK from [5] cannot generate data.) For our BIK, we provide a more detailed analysis of MAE_{int} in Supp.Mat. 7.

Regarding the prediction with uncertainty, BIK has at least 2 times better WMAE on *Load* and *Synth* $w = 25$ than with all competitors. On *Synth* $w = 50, 100, 200$ the baselines catch up a bit, but BIK still beats them by 30% less

Table 1. Evaluation metrics for different kernels and data sets. Bold entries mark the best result within one metric

Data	Kernel	Metrics $\mathbf{MSE}_{var}$	$\mathbf{MAE}_{int}$	WMAE
Synth w=25	BIK	**5.82 ± 12.**	**7.6 ± .45**	**3.79 ± 2.9**
	RBFIK	24.9 ± 25.	—	44.2 ± 60.
	BK	15.6 ± 20.	72.8 ± 4.6	6.9 ± 133
	BNK	15.6 ± 20.	73.0 ± 6.0	6.9 ± 133
Synth w=50	BIK	**5.87 ± 14.**	**3.67 ± .26**	**2.33 ± 2.0**
	RBFIK	24.6 ± 27.	—	13.5 ± 19.
	BK	20.8 ± 25.	71.1 ± 5.8	3.38 ± 42.
	BNK	20.8 ± 25.	72.4 ± 4.3	3.38 ± 42.
Synth w=100	BIK	**4.7 ± 13.**	**2.0 ± .14**	**4.35 ± 3.3**
	RBFIK	20.6 ± 25.	—	44.8 ± 62.
	BK	17.8 ± 23.	68.5 ± 5.2	5.95 ± 89.
	BNK	17.8 ± 23.	70.0 ± 4.7	5.95 ± 89.
Synth w=200	BIK	**5.41 ± 9.2**	**1.12 ± .09**	**4.27 ± 3.5**
	RBFIK	22.4 ± 19.	—	50.9 ± 71.
	BK	20.6 ± 18.	63.2 ± 5.4	5.50 ± 51.
	BNK	20.6 ± 18.	62.9 ± 4.2	5.50 ± 51.
Load	BIK	**.50 ± 1.2**	**.39 ± .006**	**.35 ± .74**
	RBFIK	.64 ± 1.6	—	3.5 ± 7.4
	BK	.66 ± 1.6	3.3 ± .07	12. ± 26.
	BNK	.56 ± 1.4	3.7 ± .08	.80 ± 1.7
HIPE	BIK	**12.5 ± 26.**	**.69 ± .031**	**0.42 ± 0.3**
	RBFIK	43.1 ± 43.	—	8.02 ± 6.5
	BK	45.5 ± 44.	5.84 ± .21	518. ± 429
	BNK	45.5 ± 44.	5.69 ± .19	476. ± 395
Stock	BIK	**1.13 ± 2.9**	**14.8 ± 1.1**	**0.32 ± 0.3**
	RBFIK	3.65 ± 5.1	—	4.48 ± 3.9
	BK	3.98 ± 5.3	63.1 ± 3.2	46k ± 38k
	BNK	3.98 ± 5.3	60.9 ± 2.6	45k ± 38k

error. Also, the WMAE variance suggests that the baselines are very unstable across data sets.

The MSE_{var} between predicted variance and actual variance during measurement on *Synth*, *HIPE*, *Stock* is 2.6 times better for BIK than any baseline. On *Load* BIK is still 10% better.

Note that the results of BK and BNK are similar on synthetic data. This similarity arises because BNK learns a noise of zero. Indeed, BNK only gives good uncertainty estimates when trained on several different observations of the same data point (or with a smaller time step). With integral measurements, such data cannot be observed, leading to BNK learning incorrect small variances.

One may also notice that the variance in predictive variance (measured with MSE_{var}) is high across the experimental runs for all kernels. This is to be expected, since by chance the ground truth is sometimes simply close to the average within the integration interval, leading to a high deviation. Even with this high deviation, MSE_{var} is still meaningful for comparing the quality of the uncertainty quantification as long as the prediction error is similar. Even though BNK estimates a similar uncertainty as BIK, the metrics MAE_{int} and WMAE show that the uncertainty estimation of BNK is useless because of its much higher prediction error.

7 Conclusions

Integrated Brownian motions are crucial in many physical processes and data collection techniques. The conventional Brownian kernel, while effective for modeling Brownian motion, falls short in capturing the uncertainties associated with integrated data.

This study has tackled modeling integrated Brownian motions precisely, by providing an analytical solution to the novel Brownian integral kernel (BIK). The BIK enables precise estimation of variance associated with the underlying quantity of interest. Further, the BIK is a valuable tool for tasks like regression with uncertainty estimation and for data synthesis partially conditioned on measurements, as shown in our experiments.

Our contributions bridge a significant gap in modeling integrated processes. Our Brownian integral kernel enhances the accuracy and reliability of Gaussian process modeling in such uncertain and dynamic environments by a factor of at least 2 on every dataset and against every baseline. Data synthesis with our integral kernel is better by a factor of at least 10 compared to all baselines.

While our Brownian integral kernel is a substantial advancement, there are avenues for further exploration: First, the challenge of concept drift, i.e., changes of behavior of the underlying ground truth stream, and how to handle it, is a relevant research direction. Additionally, investigating the properties of other integrated processes besides the Brownian integrated process could result in additional new kernels useful for modeling such processes. Finally, using our kernel in applied research could lead to advances in several directions, such as estimating privacy violations and disaggregating load data from smart meters.

Supplementary Material We include detailed notation, additional experiments, and proofs in our Supp.Mat. published on Git Hub[4].

Acknowledgments. This work was supported by the German Research Foundation (DFG) as part of the Research Training Group GRK 2153: Energy Status Data – Informatics Methods for its Collection, Analysis, and Exploitation and by the Baden-Württemberg Foundation via the Elite Program for Postdoctoral Researchers.

[4] git: https://github.com/bela127/Brownian-Integral-Kernel

This preprint has not undergone peer review or any post-submission improvements or corrections. The Version of Record of this contribution is published in "Data Science: Foundations and Applications", and is available online at: https://doi.org/10.1007/978-981-96-8295-9_8.

Disclosure of Interests. The authors have no competing interests to declare that are relevant to the content of this article.

References

1. Bischof, S., Trittenbach, H., Vollmer, M., Werle, D., Blank, T., Böhm, K.: Hipe: An energy-status-data set from industrial production. In: e-Energy. p. 599–603. ACM (2018)
2. Boyle, P.: Gaussian Processes for Regression and Optimisation. Thesis at WGTN (2007)
3. Cutsem, T., Vournas, C.: Voltage Stability of Electric Power Systems. Springer US (1998)
4. Eric, S., Maarten, S., Andreas, K.: A tutorial on gaussian process regression: Modelling, exploring, and exploiting functions. J. Math. Psychol. (2018)
5. Fariba, Y., T, S.M., Álvarez Mauricio: Multi-task learning for aggregated data using gaussian processes. In: Advances in Neural Information Processing Systems. Curran Associates, Inc. (2019)
6. Ferris, B., Hähnel, D., Fox, D.: Gaussian processes for signal strength-based location estimation. In: Robotics: Science and Systems (2006)
7. Friz, P.K., Gassiat, P., Lyons, T.: Physical brownian motion in a magnetic field as a rough path. AMS **367**, 7939–7955 (2015)
8. Gilanifar, M., Wang, H., Sriram, L.M.K., Ozguven, E.E., Arghandeh, R.: Multitask bayesian spatiotemporal gaussian processes for short-term load forecasting. IEEE Trans. Ind. Elect. (2020)
9. GPy: GPy: A gaussian process framework in python. `http://github.com/SheffieldML/GPy` (since 2012)
10. Jidling, C., Wahlström, N., Wills, A., Schön, T.B.: Linearly constrained gaussian processes. In: NIPS. vol. 30. Curran Associates, Inc. (2017)
11. Kumar, S.: 2019-2024 us stock market data (2024). `https://doi.org/10.34740/KAGGLE/DSV/7553516`
12. Kurtz, V., Lin, H.: Kalman filtering with gaussian processes measurement noise (2019)
13. Lanoiselée, Y., Briand, G., Dauchot, O.: Statistical analysis of random trajectories of vibrated disks: towards a macroscopic realization of brownian motion. Physical Review **98** (2018)
14. Li, Z., Guo, F., Chen, L., Hao, K., Huang, B.: Hybrid kernel approach to gaussian process modeling with colored noises. Comput. Chem. Eng. **143**, 107067 (2020)
15. Liu, F., Gao, Z., Yang, C., Ma, R.: Extended kalman filters for continuous-time nonlinear fractional-order systems involving correlated and uncorrelated process and measurement noises. International Journal of Control, Automation and Systems **18**, 2229–2241 (2020)
16. Longi, K., Rajani, C., Sillanpää, T., Mäkinen, J., Rauhala, T., Salmi, A., Haeggström, E., Klami, A.: Sensor placement for spatial gaussian processes with integral observations. In: UAI. vol. 124, pp. 1009–1018. PMLR (2020)

17. Meng, X., Zhang, J., Guo, H.: Quantum brownian motion model for the stock market. Physica A Stat. Mech. Appl. **452**, 281–288 (2016)
18. Mori, H., Ohmi, M.: Probabilistic short-term load forecasting with gaussian processes. In: Proceedings of the 13th International Conference on, Intelligent Systems Application to Power Systems. IEEE (2005)
19. Musicant, D.R., Christensen, J.M., Olson, J.F.: Supervised learning by training on aggregate outputs. In: ICDM. p. 252–261. IEEE (2007)
20. O'Callaghan, S., Ramos, F.: Continuous occupancy mapping with integral kernels. AAAI **25**, 1494–1500 (2011)
21. Pflugradt, N., Stenzel, P., Kotzur, L., Stolten, D.: Loadprofilegenerator: An agent-based behavior simulation for generating residential load profiles. Journal of Open Source Software **7**, 3574 (2022)
22. Purisha, Z., Jidling, C., Wahlström, N., Schön, T.B., Särkkä, S.: Probabilistic approach to limited-data computed tomography reconstruction. Inverse Problems **35**, 105004 (2019)
23. Rasmussen, C.E., Williams, C.K.I.: Gaussian processes for machine learning. Adaptive computation and machine learning, The MIT Press (2006)
24. Reece, S., Roberts, S.: An introduction to gaussian processes for the kalman filter expert. In: 2010 13th International Conference on Information Fusion. pp. 1–9 (2010)
25. Sarkka, S., Hartikainen, J.: Infinite-dimensional kalman filtering approach to spatio-temporal gaussian process regression. In: Lawrence, N.D., Girolami, M. (eds.) Proceedings of the Fifteenth International Conference on Artificial Intelligence and Statistics. Proceedings of Machine Learning Research, vol. 22, pp. 993–1001. PMLR (2012)
26. Schölkopf, B., Smola, A.J.: Learning with Kernels: Support Vector Machines, Regularization, Optimization, and Beyond. MIT (2002)
27. Settles, B.: Active Learning. Springer Cham (2012)
28. Shepero, M., der Meer, D.v., Munkhammar, J., Widén, J.: Residential probabilistic load forecasting: A method using gaussian process designed for electric load data. Applied Energy (2018)
29. Smith, M.T., Alvarez, M.A., Lawrence, N.D.: Gaussian process regression for binned data (2019)
30. Solin, A., Särkkä, S.: Hilbert space methods for reduced-rank gaussian process regression. Stat. Comput. **30**, 419–446 (2019)
31. Sun, L., Alkhatib, H., Kargoll, B., Kreinovich, V., Neumann, I.: Ellipsoidal and gaussian kalman filter model for discrete-time nonlinear systems. Mathematics **7**(12) (2019)
32. Taghvaei, A., de Wiljes, J., Mehta, P.G., Reich, S.: Kalman Filter and Its Modern Extensions for the Continuous-Time Nonlinear Filtering Problem. Journal of Dynamic Systems, Measurement, and Control **140**(3), 030904 (11 2017)
33. Tanaka, Y., Tanaka, T., Iwata, T., Kurashima, T., Okawa, M., Akagi, Y., Toda, H.: Spatially aggregated gaussian processes with multivariate areal outputs. In: NEURIPS. vol. 32. Curran Associates, Inc. (2019)
34. Tanskanen, V., Longi, K., Klami, A.: Non-linearities in gaussian processes with integral observations. In: MLSP (2020)
35. Todescato, M., Carron, A., Carli, R., Pillonetto, G., Schenato, L.: Efficient spatio-temporal gaussian regression via kalman filtering. Automatica **118**, 109032 (Aug 2020)
36. Xie, J., Dubljevic, S.: Discrete-time kalman filter design for linear infinite-dimensional systems. Processes **7**(7) (2019)

37. Xu, J., Yang, C., Zhao, J., Wu, L.: Fast modeling of realistic clouds. In: CNMT (2009)

The Brownian Integral Kernel:
A New Kernel for Modeling Integrated Brownian Motions (Supplementary Material)

Béla H. Böhnke[1][0000−0002−3779−3409] bela.boehnke@kit.edu, Edouard Fouché[2][0000−0003−0157−7648], and Klemens Böhm[1][0000−0002−1706−1913]

[1] Karlsruhe Institute of Technology (KIT) IPD, Kaiserstraße 12, Karlsruhe, 76131, Baden-Würtemberg, Germany
[2] Siemens Deutschland – Work originated while at KIT, Werner-von-Siemens-Straße 1, München, 80333, Bayern, Germany

Abstract. This document contains the supplementary materials to our work *The Brownian Integral Kernel: a New Kernel for Modeling Integrated Brownian Motions*. Here, we feature additional experiments, and visualizations useful for experts to obtain an intuition of our *Brownian integral kernel* (BKI). Further, we perform an ablation study, present the detailed proof by derivation of the BKI, and analyze its runtime. In addition to this document, we offer a Python implementation[3] of our kernel, compatible with the widely adopted GPy framework for Gaussian Process modeling. Together with the implementation, we publish all the code and data needed to reproduce our experiments.

Keywords: Integral Measurements· Learning from Aggregated Data· Integrated Brownian Motion· Gaussian Process Regression· Kernels

1 Notation

Random Variables $X, Y, Z, ...$ are denoted in uppercase, with their realizations $x, y, z, ...$ in corresponding lowercase. $X \sim \mathcal{N}(0, 1)$ signifies that X follows a standard normal distribution. As a shorthand, one can also write $x \leftarrow \mathcal{N}(0, 1)$ to express that a realization is drawn from a normal distribution.

Random Functions $F : x \mapsto F(x)$ associate each value x_i of a variable $x \in \mathbb{R}$ with a random variable $F(x_i)$ [11]. As such, a random function extends the notion of random variables to a continuous function space. *Sample Functions* $f(x) \leftarrow F(x)$ are functions $f : x \mapsto f(x)$ drawn from a random function $F(x)$.

Stochastic Processes S or random processes are random functions $S : t \mapsto S(t)$ where $t \in \mathbb{T}$ is interpreted as time, i.e., $\mathbb{T} = \mathbb{R}_+$.

[3] git: https://github.com/bela127/Brownian-Integral-Kernel

Brownian Motions $B : t \mapsto B(t)$ are stochastic processes characterized by random increments: $\delta B(\delta t) = B(t + \delta t) - B(t)$, these increments follow the normal distribution $\delta B(\delta t) \sim \mathcal{N}(0, \delta t)$. Brownian motion occurs in many scenarios where many small, random, and independent changes lead to a random overall change [11].

Gaussian Processes (GPs) are stochastic processes such as:
$GP(x) \sim \mathcal{N}(m(x), v(x))$, illustrating that the process $GP(x)$ comes from a normal distribution with mean $m(x)$ and variance $v(x)$ depending on x [11]. One often uses GPs for applications other than time series modeling, which is why x is used instead of t. For instance, [8] uses a GP as a random function, i.e., as a probabilistic prior over smooth functions, and to model functions with associated uncertainty.

Kernel Functions $k(x, x')$, also called covariance functions, can define a GP instead of using a mean and variance function. Here, x, x' are two points from the regime of the GP, and $k(x, x')$ returns the covariance of the GP according to these given points.

The Brownian Kernel $k_{ff'}(t, t') = v_b \cdot min(t, t')$, with points in time t and t' has a variance parameter v_b. It translates to the drift speed of the resulting Brownian motion [11], i.e., how fast a time series diverges from a given starting point.

Primitive Functions , also called antiderivative, commonly use upper case letters. However, to avoid overlap in notation with random functions, we will use calligraphic letters $\mathcal{F}$ to denote primitive functions. In addition, we will use index notation to denote partly integrated functions, which is required for multivariate functions. For example:
$k(t, t') = k_{ff'}(t, t')$ is the original function, $k_{\mathcal{F}f'}(t, t') = \int_s^e k_{ff'}(t, t')\delta t$ is the one time integration and $k_{\mathcal{F}\mathcal{F}'}(t, t') = \int_s^e \int_{s'}^{e'} k_{ff'}(t, t')\delta t'\delta t$ the full (two-time) integration. Indexes of a primitive function $\mathcal{F}_{t,t'}$ (denoted with a calligraphic letter) are simply used for naming and do not have any special meaning if not otherwise specified in the text.

2 Extended Discussion of Related Work

Our work focuses on modeling time-continuous processes that contain integrators and on generating data from such learned models with Gaussian process regression. Such Gaussian processes (GPs) are the typical approach for this application [3], see Algorithm 2. A key strength of GPs is their use of flexible kernel functions, which allow for modeling complex, non-linear relationships in continuous data without explicit parametric assumptions, see step 1 in Algorithm 2. After training (step 2), GPs provide a posterior distribution over functions, making it possible not only to predict outcomes (step 3) but also associated uncertainty and to generate new realistic (continuous) data (step 4). This capability is particularly valuable for simulations and uncertainty quantification. Furthermore, GPs automatically adjust their complexity based on the data, making them robust to overfitting in small datasets and scalable to larger ones, unlike methods that require fixed parametric structures, manual tuning, or large datasets [5].

Algorithm 2 Generic Use-Case of a Gaussian Processes

1: **Input:** Training data $\mathbf{t}_{\text{train}}$, $\mathbf{y}_{\text{train}}$, Test data $\mathbf{t}_{\text{test}}$
2: **Output:** Predicted mean $\mu(\mathbf{t}_{\text{test}})$, uncertainty $\sigma(\mathbf{t}_{\text{test}})$, generated data $\mathbf{y}_{\text{gen}}$
3: **Step 1: Kernel Selection**
4: Choose a kernel function $k(\cdot, \cdot)$ (e.g., RBF, Matérn, our BIK, etc., or combination).
5: **Step 2: Training**
6: Train the Gaussian process model on $\mathbf{t}_{\text{train}}$, $\mathbf{y}_{\text{train}}$ using the kernel $k(\cdot, \cdot)$.
7: Learn hyperparameters θ of the kernel by maximizing the log marginal likelihood.
8: **Step 3: Prediction and Uncertainty Estimation**
9: For test points $\mathbf{t}_{\text{test}}$, compute the posterior mean $\mu(\mathbf{t}_{\text{test}})$ and variance $\sigma^2(\mathbf{t}_{\text{test}})$ using the trained model.
10: **Step 4: Data Generation from Posterior Distribution**
11: Sample from the posterior $\mathcal{N}(\mu(\mathbf{t}_{\text{test}}), \sigma^2(\mathbf{t}_{\text{test}}))$ to generate new data $\mathbf{y}_{\text{gen}}$.

There do exist extensions of Kalman filters for time-continuous modeling [12, 23]. However, the needed time-transition functions are challenging to drive and often problem-specific. This is why the work of [10] goes so far as using GPs as a noise model for Kalman filters. Which would, in turn, require a kernel like we proposed. Further, [20,26] have shown that such Kalman filters are equivalent to Gaussian processes under certain assumptions, i.e., it is possible to transform the kernel of a GP to a transition function for a Kalman filter or even use the kernel directly in an adapted Kalman filter implementation [19].

The closest related kernel is the *Radial Basis Function (RBF)* integral kernel, introduced by [4,21]. Independently of this work [13] also derived a line-RBF integral kernel, which calculates the covariance between lines and measurements. [6] claimed that there is no analytic solution to the line-RBF integral kernel (which was disproven by [13]) and provided an approximate solution by only solving a part of the integration and solving the missing part with numeric integration. While the RBF kernel is widely used because of its universal approximation

property [14], it has no relation to actual physical processes. This questions the usefulness of its integral version. The Brownian kernel, on the other hand, directly relates to physical processes such as load profiles or market behavior.

Obtaining an integral kernel from any kernel by pure numerical integration is possible and was done for classification [15]. Similarly, in [24] a mixture of Gaussian processes and numeric integration is used to learn from spatially integrated data. However, this approach is always an approximation, and the approximation error only decreases with a quadratic number of evaluation points. Coupled with the quadratic complexity of Gaussian process regression, this becomes computationally challenging for larger datasets. Fully analytic solutions, such as ours, are superior because they only require constant calculation time and provide an exact solution to the integral [13]. [25] uses Markov chain Monte Carlo to approximate the integral during training. However, such a method requires an adaptive training strategy, preventing one from using existing Gaussian process models and standard training algorithms. We provide a more detailed analysis of training complexity in our Supp.Mat. 9.

For smooth kernels, it is feasible to approximate the integral kernel by a finite spectral approximation on a Hilbert space [7, 22]. [17] uses this approximation to solve kernel line integrals associated with the problem of x-ray tomographic reconstruction. However, the Brownian kernel is discontinuous, which renders such an approximation intractable.

3 How Kernel Integration yields an Integrated Process

Theorem 1. *The BIK $k_{\mathcal{F}\mathcal{F}'}((s,e),(s',e'))$ yields the covariance between two integral measurements $\mathcal{B}(s,e)$ and $\mathcal{B}(s',e')$ taken from a Brownian motion $b(t)$:*

$$\mathrm{Cov}[\mathcal{B}(s,e),\mathcal{B}(s',e'))] = \mathrm{Cov}[\int_s^e b(t)\delta t, \int_{s'}^{e'} b(t')\delta t']$$

.

Theorem 1 implies that the double integral over the covariance $k_{ff'}(t,t')$ of a Brownian motion $b(t)$ is equal to the covariance between two integrated measurement regions $\mathcal{B}(s,e)$ and $\mathcal{B}(s',e')$, i.e., equal to the covariance of an integrated Brownian motion:

$$\mathrm{Cov}[\int_s^e b(t)\delta t, \int_{s'}^{e'} b(t')\delta t'] = \int_{s'}^{e'}\int_s^e \mathrm{Cov}[b(t),b(t')]\delta t'\delta t.$$

[4] features a respective proof for this relation which holds for integrals of any kernel, by decomposing the covariance as $\mathrm{Cov}[X,Y] = \mathbf{E}[XY] - \mathbf{E}[X]\mathbf{E}[Y]$. An additional proof can be obtained by interchanging the sequence of integration (Fubini) [18], [1]. This also guarantees that the resulting stochastic process is again a Gaussian process.

4 Proof of BIK Correctness

Theorem 2. *The Brownian integral kernel is positive-semidefinite:*

$$\sum_{j=1}^{n}\sum_{i=1}^{n} a_i a_j k_{\mathcal{F}\mathcal{F}'}((s_i,e_i),(s_j,e_j)) \geq 0$$

for any $s_i, e_i, s_j, e_j \in \mathbb{T} | s_i < e_i, s_j < e_j$ and for any $a_i, a_j \in \mathbb{R}$.

Proof. Theorem 2 directly follows from the derivation of the BIK as an integration of an existing kernel. The well-known Brownian kernel $k_{ff'}(t,t')$ is known to be positive-semidefinite [11]. Any integral of a kernel is again a kernel [1]. Therefore, the two times integral of $k_{ff'}(t,t')$, which results in the Brownian integral kernel, is positive-semidefinite. □

5 Details on used Data Sets

- For *Synth*, we draw data from a Gaussian process with a Brownian Kernel to obtain true Brownian motion behavior. To obtain integral measurements, we integrate this data numerically by summing over given equidistant time intervals. We generate 20 such time series, each with a length of 2.5k, 5k, 10k, and 20k time steps, and integrate over a window size $w \in [25, 50, 100, 200]$ steps, respectively. This results in the constant number of 1000 integral measurements for training.
- For *Load*, we use 17 consumer load profiles with one-minute resolution and a length of 7 days (time series of the electricity consumption of households) generated with a widely used data generator [16]. This generator simulates real-world households according to 400+ parameters, such as household size, gender and age of household members, employment, photovoltaic, and many more, and is steadily improved. It is accepted as close to real-world data in the electricity community as witnessed by the citations listed in [16]. Like smart meters, we aggregate the resulting one-minute profiles in 15-minute intervals.
- For *Real*, we use real-world load profiles provided by a private household, that are already aggregated in 15-minute intervals. Here no ground truth is available, and thus we only use it for evaluating the quality of the time series generated by the GP within Supp.Mat. 6.
- For *HIPE*, we use the High-resolution Industrial Production Energy (HIPE) data set [2]. It contains readings of ten machines and the main terminal of a power-electronics production plant.
- For *Stock*, we use daily stock market prices from [9]. Weekly aggregation provides us with integrated training data.

6 Providing Intuition about the BIK by A Comparative Visualization with BK

For domain experts, it is interesting to understand in which scenarios our BIK brings benefits. In this regard, we provide intuition by visualizing and discussing the similarities and differences between a Gaussian process model (*Brown*) with the Brownian kernel (BK) and a model (*Int_Brown*) with our BIK. For brevity, we omit BNK from this visual comparison because the quantitative evaluation in Section 6 has shown that this kernel is nearly equivalent to the BK for integral measurements.

We examine the estimates and estimated variances as well as the synthesized data. For this, we visualize the fitted relation and its variance together with the integrated measurements and true underlying data, as well as generated load profiles that satisfy the conditions imposed by the observed integral measurements and the used kernel.

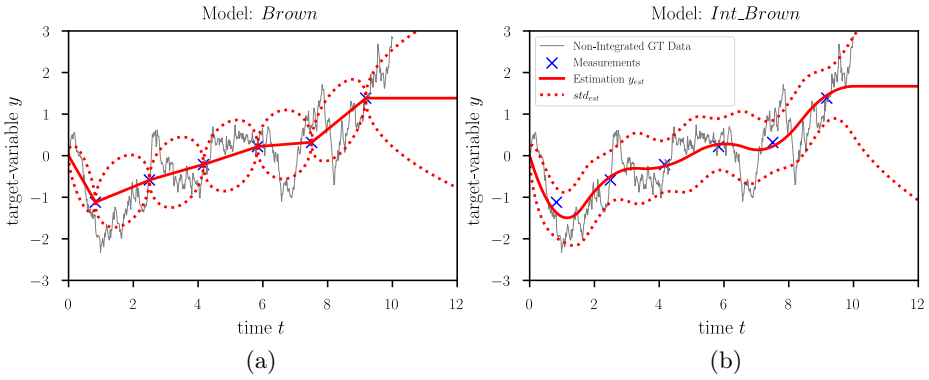

Fig. 1. Comparison between estimated variance v_{est} of the two kernels; 1a the standard Brownian kernel; 1b our new Brownian integral kernel.

Figure 1 illustrates the differences between the two models in estimation and estimation variance v_{est} (shown as a ▬ dotted line). We integrate Brownian motion data (*Synth* data), which gives us integral measurements as by definition 1 (marked as ×). These measurements are inherently imprecise due to integration.

With integral measurements, the most likely function should be a smooth function. This is because integrating over time intervals acts like a sliding window smother. Comparing the fitted functions (depicted by the ▬ line) in terms of smoothness, the *Brown* model exhibits roughness, whereas the function modeled by *Int_Brown* is smooth as expected.

Furthermore, in Figure 1a, the *Brown* model erroneously estimates a variance of zero at measurement locations, failing to account for the fact that the measurements are integrated. In contrast, *Int_Brown* with our BIK in Figure 1b

acknowledges the drift that occurs during measurement periods. It incorporates this influence by modeling the resulting inaccuracy with a higher variance. The maximum variance between measurement locations remains roughly consistent for both models. This is expected for points far away from actual measurements because the underlying Brownian motion is the same.

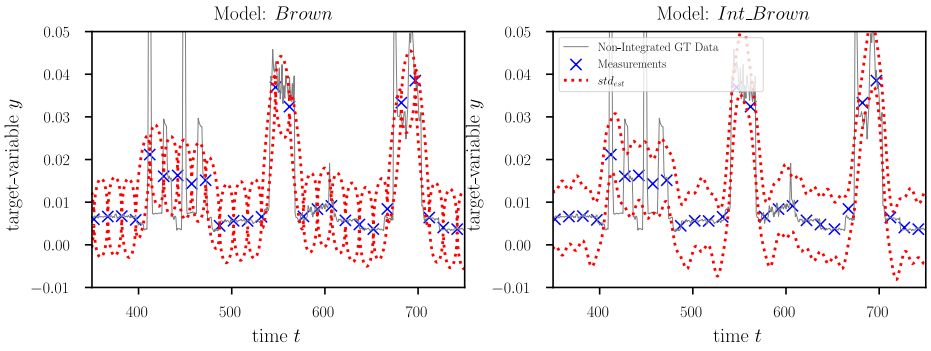

Fig. 2. Comparison using *Load* Data; 2a the Brownian kernel; 2b our new Brownian integral kernel.

In Figure 2, we observe similar patterns in the synthetic load profiles, which are integrated over 15-minute intervals (marked as ×). Additionally, we display the high-resolution ground truth (GT) load profile with a one-minute resolution (depicted by the — line). Upon comparing the actual load profile with the predicted one, it is evident that the true profile seldom aligns precisely with the integral measurement points. The *Int_Brown* model accurately captures this, exhibiting high variance in the vicinity of these locations.

In Figure 3, we see the ability of the GPs to synthesize data partially conditioned on measurements. Both models (*Brown* Figure 3a, and *Int_Brown* Figure 3b) are conditioned on the data presented in Figure 2. With *Brown*, all the generated time series pass through the measurement points (marked as ×), which is incorrect. Integrating the generated data gives random values that are not equal to the observed measurements. In contrast, *Int_Brown* correctly generates data that does not necessarily intersect with the measurement locations. The integration of this data, however, yields the correct measured value. Therefore, the data generated with our Brownian integral kernel reflects reality more accurately.

In Figure 4, we trained the models on real-world data (*Real*) and generated potential load profiles. The behavior of load profiles produced by our *Int_Brown* model, as shown in Figure 4b, is plausible, as integrating them again yields the measured data, this is not the case for data generated with *Brown*.

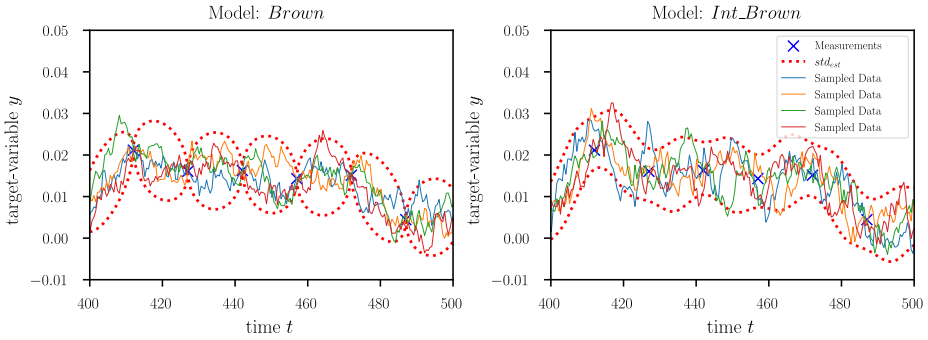

Fig. 3. Data generation from prior conditioned on *Load*; 3a data generated with Brownian kernel passes through measurement locations which is wrong; 3b data generated with our Brownian integral kernel. It does not need to go through measurement locations, but its integral is guaranteed to be the same as what was measured.

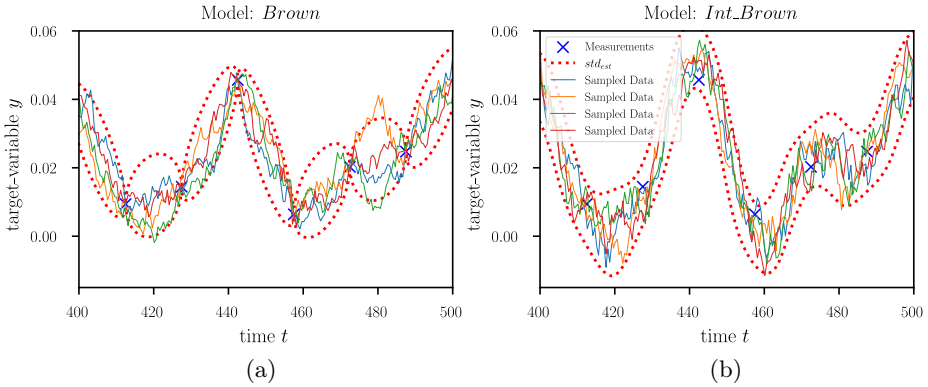

Fig. 4. Data generated from a model conditioned on real-world data (*Real*); 4a integrating data from the Brownian kernel does not reflect real behavior; 4b data from our Brownian integral kernel is much more likely in the real world, and integrating the data results in the measured data.

7 Ablation Study of Integral Window Size and Data Variance

In the following, we will examine how properties of the underlying physical process impact the estimation and the estimated uncertainty. First, we will discuss how the integral window size, i.e., the time constant of the integrator of a physical process, reflects on estimations. Secondly, we will examine the difference between Brownian motions with different variances – equivalent to different drift speeds of the Brownian motion.

7.1 Impact of the Integral Window Size

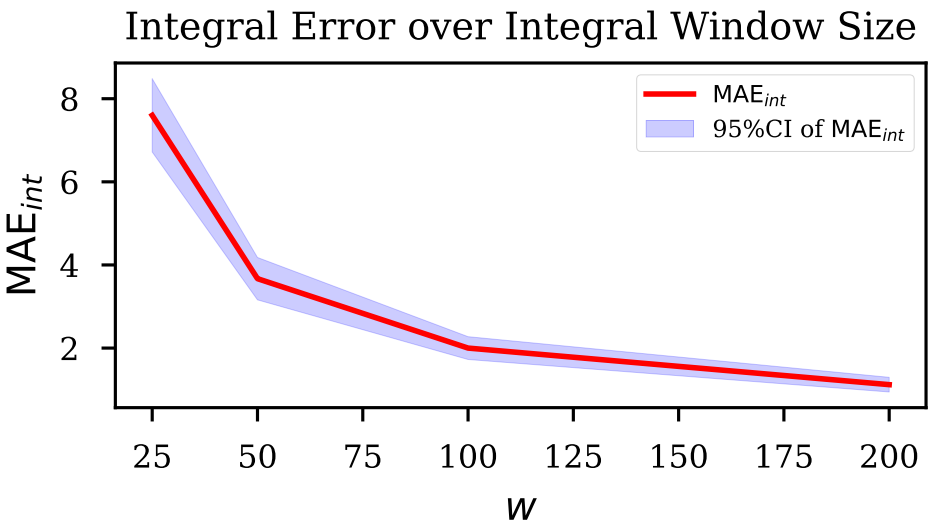

Fig. 5. Comparison of how changing the integral window size changes the integration error of generated data.

An observant reader may notice that the MAE_{int} decreases with increasing window size w. See Figure 5. We examined this behavior in depth and found that it is an artifact of the metric calculation rather than our kernel.

We calculate the metric over a fixed number of generated points in time, equal to the points provided by the original ground truth data, i.e., w points. We then sum up the values at these points to approximate the integral measurement and calculate the error in relation to the ground-truth integral. However, as the generated data is continuous, using a fixed number of points will always introduce an error in the integral approximation. The smaller the number of points, the greater the error and the larger the approximation variance (refer to the blue region in Figure 5). Indeed, in our experiments, we found that maintaining the

same start and end times for integration while increasing the number of points within the interval reduces the metric error. The error approaches zero for large w, which aligns with our expectations for an exact kernel like ours – integrating the data generated with the kernel yields the ground-truth integral value.

7.2 Impact of Data Variance

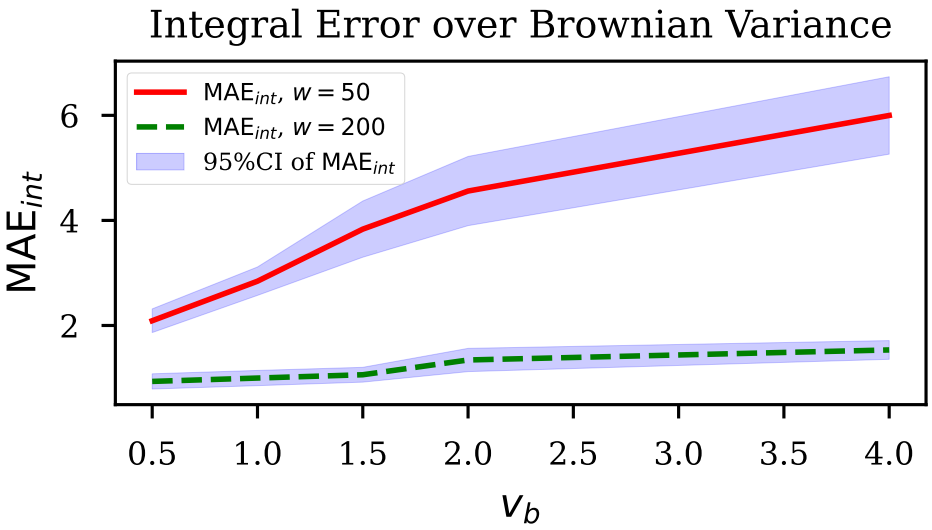

Fig. 6. Comparison of how Brownian ground truth data with different drift speeds v_b changes the integration error of generated data.

The previous observation in Supp.Mat. 7.1 has shown us that our kernel gives exact solutions for the same ground truth but with different integration intervals. Now we will examine how changing the speed of the Brownian motion, i.e., the Brownian variance v_b will impact MAE$_{int}$. In Figure 6 we see that increasing v_b while keeping $w = 50$ constant increases MAE$_{int}$. This behavior is again coused by the metric calculation. The Brownian motion within the same interval now behaves more erratically, requiring more evaluation points to calculate the integral with the same precision. Increasing the evaluation points ($w = 200$) (while keeping training points the same) again leads to a declining error approaching zero for any v_b, which is the expected behavior for an exact kernel.

8 Proof for the Brownian Integral Kernel by Derivation

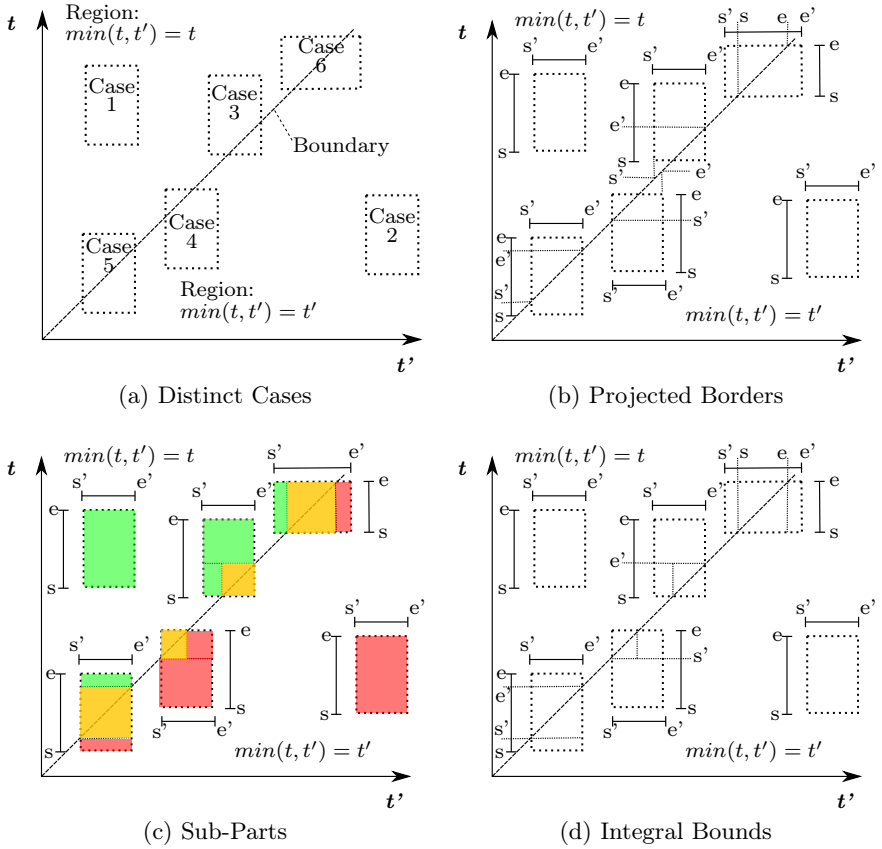

(a) Distinct Cases (b) Projected Borders

(c) Sub-Parts (d) Integral Bounds

Fig. 7. Integral case distinction; 7a The six distinct cases; 7b The projected integral borders; 7c Division of cases into (toned) sub-parts; 7d Bounds of sub-integrals

Proof. The function $min(t, t')$ is discontinuous, so the solution of the integral:

$$k_{\mathcal{F}\mathcal{F}'}((s,e),(s',e')) = v_b \cdot \int_{s'}^{e'} \int_{s}^{e} min(t,t')\delta t \delta t',$$

depends on the integration bounds s, e, s', e'. To prove Theorem 1, we need a case distinction to cover the different bound configurations. We visualize each bound configuration in Figure 7a. We do so by drawing a boundary into one quadrant where $min(t, t')$ switches from yielding t to yielding t'. This boundary is the linear function $t' = t$. In the region above the boundary, the function $min(t, t')$

yields t. In the region below, it yields t'. We then see that there are six cases of possible bound configurations (dotted boxes). Because $min(t, t')$ is symmetric to the boundary, we can project s, e, s', e' onto the other axis, receiving an ordering of the integral borders. This ordering uniquely identifies each of the six cases. See if-conditions of Theorem 1 and Figure 7b (thin lines).

We further divide these six cases into smaller partitions and find that three common sub-parts, highlighted in Figure 7c, give solutions for each partition. While the solution for the sub-parts is structurally similar, the integral bounds are different. This is why we solve each sub-part independently of the specific bounds by substituting the upper bounds with u, u' and the lower bounds with l, l'. We name the resulting three sub-integrals after the regions they are part of: Integrals with integration bounds u, u', l, l' in one region $u, u', l, l' \in \{t \mid t < t'; t, t' \in \mathbb{T}\}$ are named $\mathcal{F}_{tt}$ and in the other region $u, u', l, l' \in \{t' \mid t' < t; t, t' \in \mathbb{T}\}$ are named $\mathcal{F}_{t't'}$ respectively. Integrals with bounds in both regions are named $\mathcal{F}_{tt'}$. In Figure 7c the sub-integral $\mathcal{F}_{tt}$ has color green, $\mathcal{F}_{t't'}$ red and $\mathcal{F}_{tt'}$ orange.

Sub-parts $\mathcal{F}_{tt}$ and $\mathcal{F}_{t't'}$: The function $min(t, t')$ is continuous for these sub-parts. This allows us to directly integrate once, leading to:

$$
\begin{aligned}
t < t' : \mathcal{F}_t(t, l', u') = \int_{l'}^{u'} min(t, t')\delta t' = \int_{l'}^{u'} t\delta t' = \\
|_{t'=l'}^{u'}\ t \cdot t' = t \cdot u' - t \cdot l' \qquad (1) \\
t' < t : \mathcal{F}_{t'}(l', u') = \int_{l'}^{u'} min(t, t')\delta t' = \int_{l'}^{u'} t'\delta t' = \\
|_{t'=l'}^{u'}\ \frac{1}{2}t'^2 = \frac{1}{2}u'^2 - \frac{1}{2}l'^2 \qquad (2)
\end{aligned}
$$

We finish the first part of the proof by integrating twice, which gives us:

$$
\begin{aligned}
t < t' : \mathcal{F}_{tt}((l', u'), (l, u)) = \int_{l}^{u}\int_{l'}^{u'} t\delta t'\delta t = \\
|_{t=l}^{u}\ \frac{1}{2}t^2 \cdot u' - \frac{1}{2}t^2 \cdot l' = \frac{1}{2}u^2 \cdot u' - \frac{1}{2}u^2 \cdot l' - \frac{1}{2}l^2 \cdot u' + \frac{1}{2}l^2 \cdot l', \\
t' < t : \mathcal{F}_{t't'}((l', u'), (l, u)) = \int_{l}^{u}\int_{l'}^{u'} t'\delta t'\delta t = \\
|_{t=l}^{u}\ \frac{1}{2}u'^2 \cdot t - \frac{1}{2}l'^2 \cdot t = \frac{1}{2}u'^2 \cdot u - \frac{1}{2}l'^2 \cdot u - \frac{1}{2}u'^2 \cdot l + \frac{1}{2}l'^2 \cdot l.
\end{aligned}
$$

These are the Equations 1 and 2 of Theorem 1.

Sub-part $\mathcal{F}_{tt'}$: The third integral $\mathcal{F}_{tt'}$ needs a separate solution because it intercepts the region border and, thus, is discontinuous. We derive Equation 3 by looking at $min(t, t')$ geometrically, see Figure 8. The volume of the geometry is equivalent to the two-times integration. We decompose the geometry into two

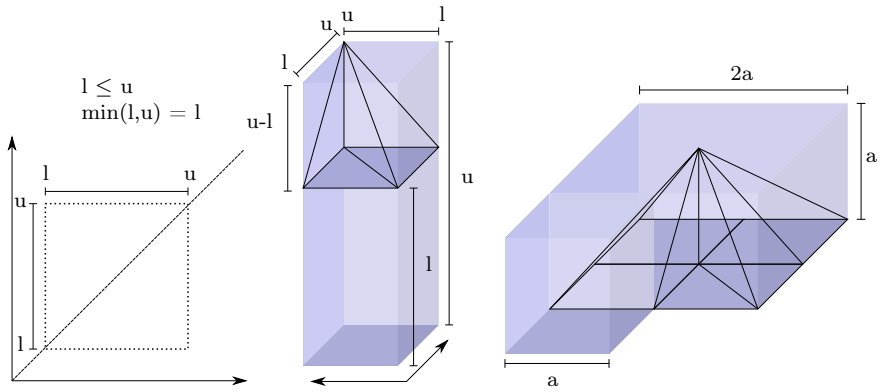

(a) Total Volume (b) Pyramid

Fig. 8. Geometric view on integrating; 8a Total volume; 8b subvolumes combined to pyramid.

subvolumes (sv), one cuboid (cub), and one more complex subvolume (com). We calculate the volume of the cuboid directly, see Figure 8a. By merging the geometry of the complex subvolume four times with itself, we obtain a pyramid, see Figure 8b. We now work out the integral bounds and obtain the solution to the double integral with the following system of equations:

$$\begin{cases} \mathrm{sv}_{com} = \frac{1}{4} V_{pyr} \\ V_{pyr} = \frac{1}{3} V_{cub} \\ V_{cub} = h \cdot w \cdot d \end{cases} \begin{cases} \Longrightarrow \\ a{=}u{-}l \\ h{=}a \\ w{=}2a \\ d{=}2a \end{cases} \begin{cases} \mathrm{sv}_{com} = \frac{1}{3}(u-l)^3 \\ \mathrm{sv}_{cub} = (u-l)^2 \cdot l \\ \mathcal{F}_{tt'}(l,u) = \mathrm{sv}_{com} + \mathrm{sv}_{cub} \end{cases},$$

which results in Equation 3 of Theorem 1:

$$\mathcal{F}_{tt'}(l,u) = \frac{1}{3}(u-l)^3 + (u-l)^2 \cdot l.$$

To combine the three subintegrals into the six original cases, we still need the integral bounds of the subintegrals corresponding to the original cases. Using the symmetric property of $min(t,t')$, we can obtain these bounds, see Figure 7d. With the matching integral bounds, we obtain the solution to the Brownian integral kernel, Theorem 1. □

9 Computational Complexity of the BIK

Concerning computational complexity, one has to distinguish between the complexity of the training algorithm without kernel and the complexity of the standalone kernel. We perform all experiments (for our kernel as well as the baseline kernels) with the standard GP model from the GPy framework[4], which has a complexity of $O(n^2)$. Depending on the use case and the needed accuracy, other less complex models can be employed to approximate GP. For example, one can use gradient-based models that allow batch training with a complexity of $O(n \cdot i)$, where i is the number of training iterations. Further, new work [19, 20, 26] has shown how to use GP kernels directly in an adapted Kalman filter implementation, thereby reducing the runtime to $O(n)$ as long as certain assumptions are met. Similarly, methods for training on time series can be used, like sliding windows that discard old measurements to keep n small, thereby losing information from old measurements. This is possible for all kernels, including ours.

If an exact solution is needed, the standard GP model with complexity $O(n^2)$ must be used. For each of these n^2 calculations, the kernel is invoked once, which is why kernel complexity can become an issue when too large. Our analytically derived BIK achieves the lowest possible complexity of $O(1)$, which makes it ideal. In comparison, the work [6] has a complexity of $O(m)$ where m are the number of Montecarlo iterations used to approximate the integral. Here, m needs to be high to obtain good approximations. While full numerical integration like in [15] and [24] is possible for any kernel, it comes with a complexity of $O(m^2)$ because of the nested Montecarlo iterations. Coupled with the quadratic complexity of Gaussian process regression, this becomes computationally challenging for larger datasets.

References

1. Abrahamsen, P.: A Review of Gaussian Random Fields and Correlation Functions. Rapport 917 (1997)
2. Bischof, S., Trittenbach, H., Vollmer, M., Werle, D., Blank, T., Böhm, K.: Hipe: An energy-status-data set from industrial production. In: e-Energy. p. 599–603. ACM (2018)
3. Eric, S., Maarten, S., Andreas, K.: A tutorial on gaussian process regression: Modelling, exploring, and exploiting functions. J. Math. Psychol. (2018)
4. Fariba, Y., T, S.M., Álvarez Mauricio: Multi-task learning for aggregated data using gaussian processes. In: Advances in Neural Information Processing Systems. Curran Associates, Inc. (2019)
5. Ferris, B., Hähnel, D., Fox, D.: Gaussian processes for signal strength-based location estimation. In: Robotics: Science and Systems (2006)
6. Hendriks, J.N., Jidling, C., Wills, A., Schön, T.B.: Evaluating the squared-exponential covariance function in gaussian processes with integral observations (2018)

[4] GPy: https://gpy.readthedocs.io

7. Jidling, C., Wahlström, N., Wills, A., Schön, T.B.: Linearly constrained gaussian processes. In: NIPS. vol. 30. Curran Associates, Inc. (2017)
8. Karvonen, T., Wynne, G., Tronarp, F., Oates, C., Särkkä, S.: Maximum likelihood estimation and uncertainty quantification for gaussian process approximation of deterministic functions. SIAM/ASA JUQ (2020)
9. Kumar, S.: 2019-2024 us stock market data (2024). https://doi.org/10.34740/KAGGLE/DSV/7553516
10. Kurtz, V., Lin, H.: Kalman filtering with gaussian processes measurement noise (2019)
11. Lindgren, G., Rootzen, H., Sandsten, M.: Stationary Stochastic Processes for Scientists and Engineers. T&F (2013)
12. Liu, F., Gao, Z., Yang, C., Ma, R.: Extended kalman filters for continuous-time nonlinear fractional-order systems involving correlated and uncorrelated process and measurement noises. International Journal of Control, Automation and Systems **18**, 2229–2241 (2020)
13. Longi, K., Rajani, C., Sillanpää, T., Mäkinen, J., Rauhala, T., Salmi, A., Haeggström, E., Klami, A.: Sensor placement for spatial gaussian processes with integral observations. In: UAI. vol. 124, pp. 1009–1018. PMLR (2020)
14. Micchelli, C.A., Xu, Y., Zhang, H.: Universal kernels. J. Mach. Learn. Res. (2006)
15. O'Callaghan, S., Ramos, F.: Continuous occupancy mapping with integral kernels. AAAI **25**, 1494–1500 (2011)
16. Pflugradt, N., Stenzel, P., Kotzur, L., Stolten, D.: Loadprofilegenerator: An agent-based behavior simulation for generating residential load profiles. Journal of Open Source Software **7**, 3574 (2022)
17. Purisha, Z., Jidling, C., Wahlström, N., Schön, T.B., Särkkä, S.: Probabilistic approach to limited-data computed tomography reconstruction. Inverse Problems **35**, 105004 (2019)
18. Rasmussen, C.E., Williams, C.K.I.: Gaussian processes for machine learning. Adaptive computation and machine learning, The MIT Press (2006)
19. Reece, S., Roberts, S.: An introduction to gaussian processes for the kalman filter expert. In: 2010 13th International Conference on Information Fusion. pp. 1–9 (2010)
20. Sarkka, S., Hartikainen, J.: Infinite-dimensional kalman filtering approach to spatio-temporal gaussian process regression. In: Lawrence, N.D., Girolami, M. (eds.) Proceedings of the Fifteenth International Conference on Artificial Intelligence and Statistics. Proceedings of Machine Learning Research, vol. 22, pp. 993–1001. PMLR (2012)
21. Smith, M.T., Alvarez, M.A., Lawrence, N.D.: Gaussian process regression for binned data (2019)
22. Solin, A., Särkkä, S.: Hilbert space methods for reduced-rank gaussian process regression. Stat. Comput. **30**, 419–446 (2019)
23. Taghvaei, A., de Wiljes, J., Mehta, P.G., Reich, S.: Kalman Filter and Its Modern Extensions for the Continuous-Time Nonlinear Filtering Problem. Journal of Dynamic Systems, Measurement, and Control **140**(3), 030904 (11 2017)
24. Tanaka, Y., Tanaka, T., Iwata, T., Kurashima, T., Okawa, M., Akagi, Y., Toda, H.: Spatially aggregated gaussian processes with multivariate areal outputs. In: NEURIPS. vol. 32. Curran Associates, Inc. (2019)
25. Tanskanen, V., Longi, K., Klami, A.: Non-linearities in gaussian processes with integral observations. In: MLSP (2020)

26. Todescato, M., Carron, A., Carli, R., Pillonetto, G., Schenato, L.: Efficient spatio-temporal gaussian regression via kalman filtering. Automatica **118**, 109032 (Aug 2020)